

Figure 1. The fabrication process of DNA–SWNT electrode. First, ssDNA was mixed with SWNT to form DNA–SWNT hybrid, and then, the DNA–SWNT hybrids were deposited onto a glass substrate to form a uniform film, and finally, the film was welded with copper wire and mounted with resin, leaving a small nanotube area for sensing.

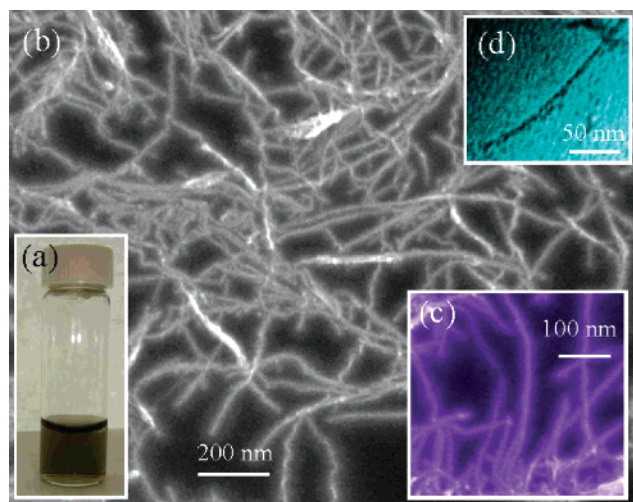


Figure 2. Images of DNA–SWNT hybrids. (a) Pictures of well-solubilized DNA–SWNT solution; (b) SEM image of individually dispersed SWNTs; (c) enlarged SEM image; (d) TEM image, which clearly shows the shape of DNA wrapping on SWNTs.

The thickness of the final film of dried ssDNA–SWNTs is about 7 μm (measured by SEM from side view), and resistivity of the film is 45.18 $\Omega\text{ cm}$ (measured by four probe method).

A working electrode was made by welding a copper wire onto the ssDNA–SWNTs film, with silver paste. After this, the electrode was partly mounted with epoxy resin, and a small area of film ($\sim 0.142\text{ cm}^2$) was left exposed, which was used to measure the voltammetric properties of the electrode, as well as to detect dopamine. The whole process to make the electrode is shown in Figure 1.

Cyclic voltammetric measurements were performed in a three-electrode system, including the ssDNA–SWNTs working electrode, a platinum counter electrode and an SCE reference electrode. The data were recorded with an EG&G 273A potentiostat/galvanostat interfaced with a computer. All of the reagents are of analytical purity as supplied by Sigma-Aldrich, and deionized water obtained from a Millipore water system was used throughout. All of the electrochemical experiments were performed at room temperature ($\sim 23\text{ }^\circ\text{C}$).

3. Results and Discussion

Purified DNA–SWNTs can be dispersed in water and form a stable solution, as shown in Figure 2a. SEM analysis indicated that SWNTs were thoroughly dispersed and existed in individual nanotubes (Figure 2b), with an average length of about 600 nm.

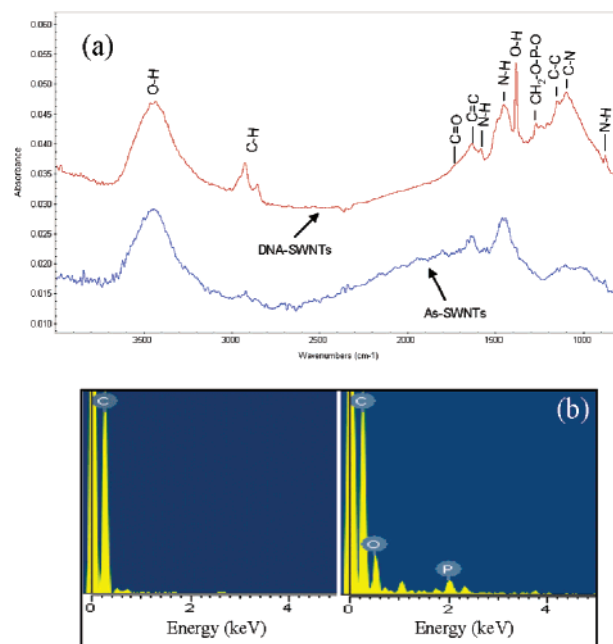


Figure 3. (a) FT-IR spectra and (b) EDS of as-produced SWNTs and DNA–SWNT hybrids.

A higher-magnification image showed a bead-string-like structure of SWNTs, indicating the wrapping of DNA along SWNT sidewalls (Figure 2c,d).

The mechanism of dispersing SWNTs by DNA can be explained by electrostatics of the DNA–SWNT hybrids. Though carbon nanotubes are electrically neutral, DNA carries lots of negative charges. So, when individual nanotubes are released by sonication, DNA binding through π -stacking charge up the nanotubes. As a result, individual nanotubes will repel each other and form a stable solution, rather than aggregating together by Van de Waals force.

To further demonstrate binding of DNA with SWNTs, FT-IR spectroscopy and EDS analyses were conducted. Figure 3a shows FT-IR spectra of bare and DNA-wrapped SWNTs. For the DNA-wrapped SWNTs sample, the peak at 1264 cm^{-1} refers to the $\text{CH}_2\text{—O—P—O}$ phosphate group.¹⁹ The DNA–SWNTs complex results in the intensity increase or the appearance of H-bonded O–H and N–H stretching vibration as well as an asymmetrical PO_2^- vibration at 1234 cm^{-1} , a sugar vibration at 880 cm^{-1} , the C=C vibration at 1640 cm^{-1} , and the C=O vibration at 1720 cm^{-1} , which indicate the helix interaction of DNA with SWNT.²⁰ The EDS analysis (Figure 3b) further confirms the existence of DNA on the SWNTs.

We found that the DNA–SWNTs hybrid could firmly attach onto a glass substrate and form a uniform film, as depicted in Figure 4. This is due to the high dispersivity of DNA–SWNTs. After dispersion, the individual SWNTs have a high surface-to-volume ratio and surface free energy, so they tend to interact with each other as well as the glass substrate to release some of the free energy while the water evaporates. The strains among any of the nanotubes to form the film are equivalent in all directions, since they are individually suspended in water. If the nanotubes are not individually suspended in water, the asymmetric strain from nanotubes will result in uneven film, which cannot adhere tightly to the glass and will easily fall off when put into solution.

The potential window is one of the most important factors for an electroanalytic electrode, and well-performing electrodes can give a good signal-to-noise ratio with a flat and wide

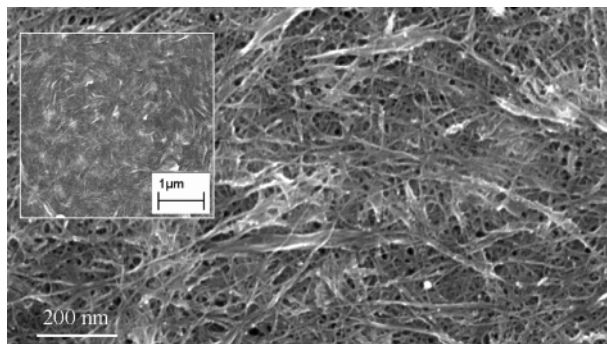


Figure 4. Topography SEM image of the ssDNA-SWNT electrode.

potential window. Figure 5a indicates that the potential window of the DNA-SWNT electrode in 0.1 M KCl is flat and wide; although the background current is a little high, no redox reaction appears in the potential window, implying this electrode may have a higher signal-to-background ratio for analytic detection.

Redox pairs are usually used to probe the quality of the electrode by cyclic voltammetry.^{21–23} To investigate the electronic transfer properties of the DNA-SWNT electrode, we chose $\text{Fe}(\text{CN})_6^{4-}/\text{Fe}(\text{CN})_6^{3-}$ as redox pairs for their voltammetric responses. In Figure 5b, the cyclic voltammograms exhibit well-defined redox reaction at potentials of 0.297 and 0.177 V. The voltammograms are reproducible, except for the first cycle, because the starting concentration distribution of reductive/oxidative reactant near the electrode is a little different from the following cycles. From Figure 5c, we can see the peak currents increase linearly with $\text{Fe}(\text{CN})_6$ concentration, which matches the equations $I_{\text{pa}} = 54.75 + 20.76 C$, $r = 9999$, and $I_{\text{pc}} = 67.05 + 18.35 C$, $r = 9997$, where $I_{\text{pa}}/I_{\text{pc}}$, C and r are the oxidation/reduction peak current in microamperes, concentration in millimoles, and correlative coefficient, respectively. We then

tried different scan rates to see what factor controls the speed of the redox reaction process. As shown in Figure 5d, both oxidation and reduction peak currents are proportional to the square root of the scan rate, $I_{\text{pa}} = -86.35 + 2587.99v^{1/2}$, $r = 9991$, and $I_{\text{pc}} = -136.95 + 2701.86v^{1/2}$, $r = 9996$, where v refers to scan rate in volts per second, indicating that the diffusion speed of $\text{Fe}(\text{CN})_6^{4-}/\text{Fe}(\text{CN})_6^{3-}$ determines the speed of the redox reaction in 1 M KCl. The electron transfer speed at the interface between the electrode and the solution is faster than that of diffusion of the reactant. From all of the analyses above, we can conclude that the redox reaction of $\text{Fe}(\text{CN})_6^{4-}/\text{Fe}(\text{CN})_6^{3-}$ in 1 M KCl is a quasi-reversible reaction.²³ Another advantage we found is that there is no foul on the surface of the electrode, because voltammograms are reproducible without any special pretreatment before each experiment, except rinse with water. It is a very important property for a DNA-SWNT electrode to be used in electrochemical analysis, because the surface of bulk carbon electrodes can usually become deactivated as a function of time when they are exposed to the laboratory atmosphere or working solution. The problem will become more severe when a biological sample is used.

To explore the potential applications of the DNA-SWNT electrode in electrochemical detection, we used low-concentration dopamine (DA) to test its selectivity and sensitivity. DA is an important neurotransmitter,²⁵ and it coexists in the interstitial fluid in the brain with ascorbic acid (AA). The physiological concentration of AA is much higher than that of DA, and the oxidation potential of the AA is close to that of DA, making selective detection of DA a challenging task. Various modified traditional electrodes have been attempted^{26,27} to address this issue, such as glassy carbon electrode, graphite electrode, and noble metal electrode. However, these electrodes usually need complicated pretreatment and modification of the electrode surface chemistry to enhance selectivity and sensitivity. In

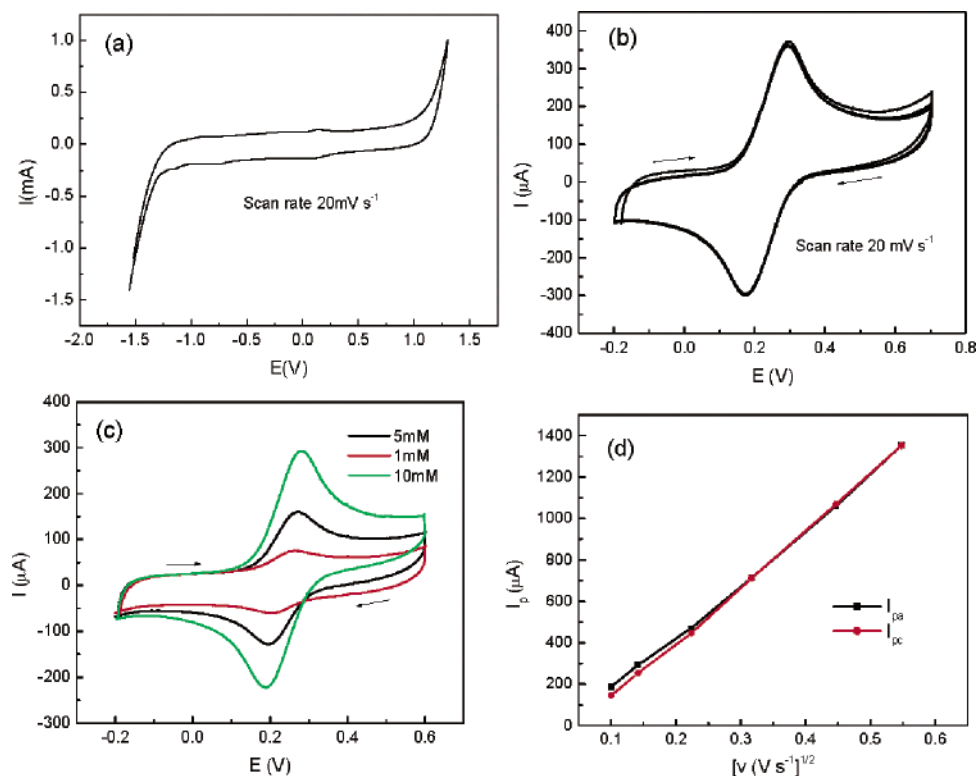


Figure 5. (a) Potential window for ssDNA-SWNT electrode in 0.1 M KCl. (b) Cycle voltammogram of 10 mM $\text{Fe}(\text{CN})_6$ in 1 M KCl for 5 cycles. (c) Cyclic voltammograms for different concentrations of $\text{Fe}(\text{CN})_6$ in 1 M KCl at scan rate of 20 mV s^{-1} . (d) Redox peak currents proportional to square root of the scan rate for 10 mM $\text{Fe}(\text{CN})_6$ in 1 M KCl.

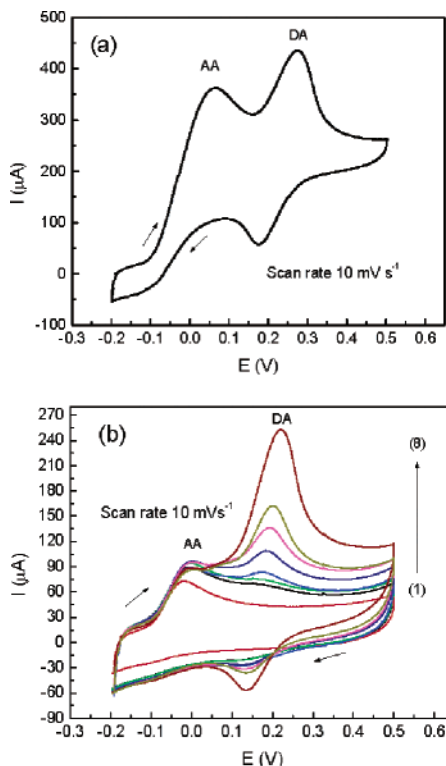


Figure 6. Cyclic voltammetric detection at DNA-SWNT electrode in 0.1 M PBS, pH 7.0 (a) for 2 mM DA + 20 mM AA and (b) for different DA concentration: (1) 0 M, (2) 5×10^{-8} M, (3) 5×10^{-7} M, (4) 5×10^{-6} M, (5) 1×10^{-5} M, (6) 5×10^{-5} M, (7) 1×10^{-4} M, (8) 5×10^{-4} M, in 2 mM AA + 0.1 M PBS, pH 7.0.

addition, some of them tend to lose stability and selectivity during measurement, and some of them do not produce well-resolved voltammograms.²⁸

Figure 6 shows results of voltammetric detection of DA using our DNA-SWNT electrode in 0.1 M phosphate buffer solution (PBS) of pH = 7.0. Peaks for DA and AA can be clearly identified at 0.273 and 0.063 V respectively, with peak separation of 0.21 V from Figure 6a. The change of peak current versus the concentration of DA can be distinguished, while the concentration of AA is kept constant, as shown in Figure 6b. The logarithmic linear fit of DA peak current versus concentration is different from lower concentration to higher concentration, which is $\log I_p (\mu\text{A}) = 2.13 + 0.04 \log C (\text{M})$, $r = 0.999$, in 10^{-6} – 10^{-8} M and $\log I_p (\mu\text{A}) = 2.99 + 0.2 \log C (\text{M})$, $r = 0.995$, in 10^{-5} – 10^{-3} M. However, the detection limit of DA can reach as low as 5.0×10^{-8} M, demonstrating highly selective and sensitive detection of DA by cyclic voltammetry.

The electron transfer of reactants during electro-oxidation is mainly determined by the conductivity of electrode material as well as the active functional groups on its surface. Owing to their excellent conductivity, metals (such as platinum and gold), glass carbon, and graphite are the materials usually used for electrodes. However, the number of active functional groups on surfaces of these materials is limited, as a result of limited exposed area on electrode surface. For the SWNT electrode, though its conductivity is not as good as that of those materials mentioned above, it has much higher surface area, which can accommodate much more active functional groups in a given region. This will significantly enhance the rate of surface-catalyzed reaction, which is proportional to surface coverage of functional groups.²⁹ For a DNA-SWNT electrode, the length of SWNTs will also play a role in conductivity. Shorter SWNTs will form more contacts, hence producing a higher contact

resistivity. In this paper, the SWNTs have an average length of 600 nm and the electrode has a resistivity of 45.18 Ω cm. Further studies are being carried out to see the effects of SWNT length on conductivity of the DNA-SWNT electrode.

DNA is rich in active functional groups, such as amino groups, carbonyl groups, and carboxyl groups; these groups can act as media for electron transfer in redox reaction and catalyze the oxidation of DA and AA.³⁰ As a result, the two anodic peak potentials of DA and AA are well-separated, indicating high selectivity and sensitivity of the DNA-SWNT electrode.

4. Conclusion

The thoroughly dispersed single-walled carbon nanotubes have been obtained by wrapping with ssDNA. The DNA-SWNT hybrids can be made into a uniform film, which firmly attaches onto glass substrate. With such advantages, we can fabricate a DNA-SWNT electrode and use it in solution phase. Electrochemical experiments indicated that the DNA-SWNT electrode possesses a flat and wide potential window, well-defined quasi-reversible voltammograms, and quick electron transfer for $\text{Fe}(\text{CN})_6^{4-}/\text{Fe}(\text{CN})_6^{3-}$, suggesting it can be used as an electrode for electrochemical analysis. Detection of a low concentration of dopamine further demonstrates high selectivity and sensitivity of this DNA-SWNTs electrode. This study opens a new application for DNA-functionalized SWNTs.

Acknowledgment. This work has been funded by NSFC (60376032), NSF, and DARPA.

References and Notes

- Baughman, R. H.; Zakhidov, A. A.; De Heer, W. A. *Science* **2002**, 297, 787.
- Charlier, J. C.; De Vita, A.; Blase, X.; Car, R. *Science* **1997**, 275, 647.
- Li, D. C.; Dai, L. M.; Huang, S. M.; Mau, A. W. H.; Wang, Z. L. *Chem. Phys. Lett.* **2000**, 316, 349.
- Frank, S. P.; Poncharal, P.; Wang, Z. L.; De Heer, W. A. *Science* **1998**, 280, 1744.
- Poncharal, P.; Wang, Z. L.; Ugarte, D.; De Heer, W. A. *Science* **1999**, 283, 1513.
- Regan, B. C.; Aloni, S.; Ritchie, R. O.; Dahmen, U.; Zettl, A. *Nature (London)* **2004**, 248, 924.
- Kong, J.; Franklin, N. R.; Zhou, C. W.; Chapline, M. G.; Peng, S.; Cho, K.; Dai, H. J. *Science* **2000**, 287, 622.
- Fennimore, A. M.; Yuzvinsky, T. D.; Han, W. Q.; Fuhrer, M. S.; Cumings, J.; Zettl, A. *Nature (London)* **2003**, 424, 408.
- De Heer, W. A.; Bonard, J. M.; Fauth, K.; Châtelain, A.; Ugarte, D.; Forró, L. *Adv. Mater.* **1997**, 9, 87.
- Chen, R. J.; Bangsaruntip, S.; Drouvalakis, K. A.; Kam, N. W. S.; Shim, M.; Li, Y.; Kim, W.; Utz, P. J.; Dai, H. J. *PNAS* **2003**, 100, 4984.
- Chen, J.; Mark, H. A.; Hu, H.; Chen, Y. S.; Rao, A. M.; Eklund, P. C.; Haddon, R. C. *Science* **1998**, 282, 95.
- Strano, M. S.; Dyke, C. A.; Usrey, M. L.; Barone, P. W.; Allen, M. J.; Shan, H. W.; Kittrell, C.; Hauge, R. H.; Tour, J. M.; Smalley, R. E. *Science* **2003**, 301, 1519.
- Shim, M.; Shi Kam, N. W.; Chen, R. J.; Li, Y. M.; Dai, H. J. *Nano Lett.* **2002**, 2, 285.
- Mickelson, E. T.; Chiang, I. W.; Zimmerman, J. L.; Boul, P. J.; Lozano, J.; Liu, J.; Smalley, R. E. *J. Phys. Chem.* **1999**, 103, 4318.
- Yanagi, H.; Mukai, H.; Ikuta, K.; Shibutani, T.; Kamikado, T.; Yokoyama, S.; Mashiko, S. *Nanotechnology* **2002**, 13, 601.
- Zheng, M.; Jagota, A.; Semke, E. D.; Santos, A. P.; Barone, P.; Chou, S. G.; Diner, B. A.; Dresselhaus, M. S.; McLean, R. S.; Onoa, G. B.; Samsonidze, G. G.; Semke, E. D.; Usrey, M. Walls, D. J. *Science* **2003**, 302, 1545.
- Keren, K.; Berman, R. S.; Buchstab, E.; Sivan, U.; Braun, E. *Science* **2003**, 302, 1380.
- Zheng, M.; Diner, B. A. *J. Am. Chem. Soc.* **2004**, 126, 15490.
- Buzaneva, E.; Karlash, A.; Yakovkin, K.; Shtogun, Y. *Mater. Sci. Eng.* **2002**, C19, 41.
- Dovbeshko, G. I.; Repnytska, O. P.; Obratsova, E. D.; Shtogun, Y. V. *Chem. Phys. Lett.* **2003**, 372, 432.
- Xu, J.; Granger, M. C.; Chen, Q. *Anal. Chem.* **1997**, 69, 591A.
- Galizzioli, D.; Trasatti, S. *J. Electroanal. Chem.* **1973**, 44, 367.

- (23) Notsu, H.; Fukazawa, T.; Tatsuma, T.; Tryk, D. A.; Fujishima, A. *Electrochem. Solid State Lett.* **2001**, *4*, H1.
- (24) Bard, A. J.; Faulkner, L. R. *Electrochemical Methods*; John Wiley & Sons: New York, 2001.
- (25) Zen, J. M.; Chen, I. L. *Electroanalysis* **1997**, *7*, 537.
- (26) Fujishima, A.; Rao, T. N.; Popa, E.; Sarada, B. V.; Yagi, I.; Tryk, D. A. *J. Electroanal. Chem.* **1999**, *473*, 179.

- (27) Miyazaki, K.; Matsumoto, G.; Yamada, M.; Yasui, S.; Kaneko, H. *Electrochim. Acta* **1999**, *44*, 3809.
- (28) Jaegfeldt, H. *J. Electroanal. Chem.* **1980**, *110*, 295.
- (29) Evans, J. F.; Kuwana, T.; Henne, M. T.; Royer, G. P. *J. Electroanal. Chem.* **1977**, *80*, 409.
- (30) Palmisano, F.; Malitesta, C.; Centonzet, D.; Bmbonin, P. Q. *Anal. Chem.* **1995**, *67*, 2207.